



저작자표시-비영리-변경금지 2.0 대한민국

이용자는 아래의 조건을 따르는 경우에 한하여 자유롭게

- 이 저작물을 복제, 배포, 전송, 전시, 공연 및 방송할 수 있습니다.

다음과 같은 조건을 따라야 합니다:



저작자표시. 귀하는 원저작자를 표시하여야 합니다.



비영리. 귀하는 이 저작물을 영리 목적으로 이용할 수 없습니다.



변경금지. 귀하는 이 저작물을 개작, 변형 또는 가공할 수 없습니다.

- 귀하는, 이 저작물의 재이용이나 배포의 경우, 이 저작물에 적용된 이용허락조건을 명확하게 나타내어야 합니다.
- 저작권자로부터 별도의 허가를 받으면 이러한 조건들은 적용되지 않습니다.

저작권법에 따른 이용자의 권리는 위의 내용에 의하여 영향을 받지 않습니다.

이것은 [이용허락규약\(Legal Code\)](#)을 이해하기 쉽게 요약한 것입니다.

[Disclaimer](#)

공학석사 학위논문

혈관 형성 촉진을 위한
일산화질소와 황화수소 동시 방출
나노입자의 개발

Development of co-delivery nanoparticles
containing nitric oxide and hydrogen sulfide
for enhanced angiogenesis

2021년 8월

서울대학교 대학원

융합과학부 나노융합전공

이 지 은

혈관 형성 촉진을 위한
일산화질소와 황화수소 동시 방출
나노입자의 개발

Development of co-delivery nanoparticles
containing nitric oxide and hydrogen sulfide
for enhanced angiogenesis

지도 교수 이강원

이 논문을 공학석사 학위논문으로 제출함
2021년 7월

서울대학교 대학원
융합과학부 나노융합전공
이지은

이지은의 공학석사 학위논문을 인준함
2021년 7월

위원장 _____ 박원철 _____

부위원장 _____ 이강원 _____

위원 _____ 송윤규 _____

Abstract

Development of co-delivery nanoparticles containing nitric oxide and hydrogen sulfide for enhanced angiogenesis

Jieun Lee

Program in Nano Science and Technology

The Graduate School of Convergence Science and

Technology

Seoul National University

Nitric oxide (NO) and hydrogen sulfide (H₂S) have been the focus of research as therapeutic agents because of their biological functions. The controlled release of NO and H₂S can enhance NO-induced angiogenesis by H₂S inhibiting PDE5A. Polymeric carriers have been researched to deliver gasotransmitters and used as therapeutic agents because of their important ability to help control the concentration of NO and H₂S. Here, NO/H₂S-releasing nanoparticles were self-assembled

from carboxyl-functionalized mPEG-PLGH-thiobenzamide [(methoxy poly (ethylene glycol-*b*-lactic-*co*-glycolic-*co*-hydroxymethyl propionic acid)-thiobenzamide)], PTA copolymer and encapsulated diethylenetriamine NONOate (DETA NONOate). The PTA copolymers were characterized by FT-IR and ¹H NMR, and the PTA-NO nanoparticles (PTA-NO-NPs) were confirmed to have core-shell structures with a size of about 140 nm. The PTA-NO-NPs were demonstrated to be biocompatible with viabilities above 100% in various cell types, with a sustained NO and H₂S releasing behavior over 72 h. Co-releasing NO and H₂S accelerated tube formation by HUVECs compared to the only NO- or H₂S-releasing groups *in vitro*. Also, PTA-NO-NPs performed enhanced angiogenesis compared to the control groups with statistically significant differences *ex vivo*. These results indicate the feasibility of medical applications through NO and H₂S crosstalk.

Keywords: nitric oxide, hydrogen sulfide, functionalized mPEG-PLGA, co-releasing nanoparticle, enhanced angiogenesis

Student Number: 2019-21580

Table of Contents

| | |
|--|-----|
| Abstract..... | I |
| Table of Contents..... | III |
| List of Tables and Figures..... | V |
| | |
| Chapter 1. Introduction..... | 1 |
| | |
| Chapter 2. Results and Discussion..... | 7 |
| 2.1 Characterization of mPEG-PLGH and mPEG-PLGH- thiobenzamide..... | 7 |
| 2.2 Characterization of PTA-NO-NPs..... | 8 |
| 2.3 Release measurement of NO and H ₂ S..... | 10 |
| 2.4 <i>In vitro</i> cytotoxicity of PTA-NO-NPs..... | 14 |
| 2.5 Angiogenic potential of PTA-NO-NPs..... | 20 |
| | |
| Chapter 3. Experimental..... | 25 |
| 3.1 Materials..... | 25 |
| 3.2 Preparation of mPEG-PLGH copolymers (Carboxyl- functionalized mPEG-PLGA)..... | 26 |
| 3.3 Preparation of mPEG-PLGH-thiobenzamide (PTA) copolymers..... | 27 |

| | |
|--|-----------|
| 3.4 Preparation of PTA nanoparticles with DETA NONOate (PTA-NO-NPs) | 28 |
| 3.5 Characterization of mPEG-PLGH and PTA copolymers | 29 |
| 3.6 Characterization of size distribution and morphology of PTA-NO-NPs..... | 29 |
| 3.7 Entrapment efficiency measurement of PTA-NO-NPs | 30 |
| 3.8 NO release measurement..... | 31 |
| 3.9 H ₂ S release measurement..... | 32 |
| 3.10 <i>In vitro</i> cytotoxicity measurement | 33 |
| 3.11 Tube formation assay | 34 |
| 3.12 Aortic ring assay | 35 |
| 3.13 Statistical analysis..... | 36 |
| | |
| Chapter 4. Conclusions | 37 |
| | |
| References | 38 |
| | |
| 국문 초록..... | 45 |

List of Tables and Figures

Figure 1. Schematic illustration of NO & H₂S co-delivery from self-assembled PTA nanoparticles for enhancing angiogenesis and synthesis scheme of mPEG-PLGH and PTA copolymers.

Figure 2. Characterization of PTA copolymers and PTA-NO-NPs.

Figure 3. *In vitro* cytotoxicity measurement of HUVECs and 3T3-L1.

Figure 4. Endothelial cell tube formation assay to assess the angiogenic potential of PTA-NO-NPs *in vitro*.

Figure 5. *Ex vivo* aortic ring assay using rat aorta.

Table S1. Molecular weight of mPEG-PLGH and PTA copolymers.

Figure S1. *In vitro* cytotoxicity measurement by CCK-8 assay of cancer cell lines (A549, C6, MCF7) and ADSCs.

Figure S2. Fluorescence images by Live/Dead assay of cancer cell lines (A549, C6, MCF-7) and ADSCs.

Chapter 1. Introduction

Gaseous signaling molecules (i.e., gasotransmitters) have emerged in therapeutics as physiological modulators because they can freely permeate membranes and regulate physiological pathways and cell functions.^{1,2} Gasotransmitters can be endogenously synthesized by various types of cells, interacting with each other in just a blip. The first identified gasotransmitter was nitric oxide (NO), which has been researched in cardiovascular systems, neuronal systems, immune modulators, wound healing, and cancer therapy.³ Hydrogen sulfide (H₂S) is also involved in various systems of mammalian physiology and is considered one of the most important signaling molecules. NO and H₂S are endogenously produced in concentrations of 5 nM–4 μM and 0.7–3 μM, respectively.^{4–6} Both gas molecules mediate specific physiological functions based on their concentration, such as vascular signaling in low concentration and apoptosis signaling in high concentration. These molecules share signaling pathways by interacting dependently or independently to modulate angiogenesis, vascular vasodilation, immune response, etc.^{7–9} Therefore, their combinatorial use could represent a

promising therapeutic agent.

NO is endogenously produced by NO synthase, and NO synthase can be activated by H₂S production, which results in increased NO levels. Endogenously produced NO converts guanosine triphosphate (GTP) to cyclic guanosine monophosphate (cGMP), and it stimulates protein kinase G (PKG). Similarly, H₂S participates in these cascade reactions by inhibiting cGMP-specific phosphodiesterase type 5 (PDE5A), which can degrade cGMP. These NO and H₂S interactions allow increased cGMP levels, which lead to a sufficient stimulation of PKG. PKG provides the signals to regulate several physiological functions, such as angiogenesis and vasodilation through controlling ion channels.¹⁰ In addition, both NO and H₂S can activate K_{ATP} channels involved in angiogenesis. From these simultaneous actions, NO signals inducing angiogenesis can be ultimately amplified by H₂S.^{11,12}

Since endogenously synthesized gasotransmitters have a short half-life and the direct administration of gas molecules carries a risk of overdose, the development of donor materials is necessary to deliver exogenously.^{13,14} Various NO or H₂S donor materials, such as releasing moieties (N-diazeniumdiolate, S-nitrosothiol, and peroxyxynitrate for NO release, and arylthioamide,

1,2-dithiole-3-thiones, and Lawessons' reagent derivatives for H₂S release), have been developed for exogenous delivery *in vivo*.¹⁵⁻¹⁹ In particular, diethylenetriamine NONOate (DETA NONOate), which is one of the derivatives of N-diazeniumdiolate, releases two NO products with proton-triggered NO-releasing mechanisms.²⁰ DETA NONOate was reported to have angiogenic potentials by controlling the release rates via vehicles,^{21,22} while 4-aminothiobenzamide, one of the arylthioamide derivatives, was reported to be a new promising therapeutic agent for cardiovascular diseases with vascular effects. Arylthioamide derivatives have showed thiol-triggered H₂S-releasing properties, such as L-cysteine, but no precise thiol-triggering mechanism has been revealed yet.²³ Also, 4-aminothiobenzamide has exhibited the advantages of a slow and sustained H₂S release as well as having easy conjugation properties.²⁴

By designing hybrid materials with the dual release of NO and H₂S, researchers can take advantage of a signal amplification of the NO signals. The hybrid molecules, such as NOSH-aspirin (NBS 1120) and ZYZ-803, have been reported.^{25,26} For delivering NO and H₂S donor materials, the modification of polymers is one of the most promising strategies. The grafting

of releasing moieties in the polymer backbone has been reported, such as poly (vinyl alcohol), poly (ethyleneimine), chitosan, alginate, and peptide-based hydrogels.²⁷⁻²⁹ Notably, the copolymer poly (ethylene glycol) (PEG) and poly (lactic-co-glycolic acid) (PLGA) is one of the most common biocompatible and biodegradable materials used in commercial therapeutics and clinical applications. With these great characteristics of copolymers, chemical functionalization expands their versatile applications, such as in drug delivery, hydrogels, and engineered scaffolds.³⁰⁻³² For instance, 2,2-bis(hydroxymethyl) propionic acid (HMPA) allows carboxyl-functionalization during the polymerization of lactic acid and glycolic acid. Poly (lactic-co-glycolic-co-hydroxymethyl propionic acid), PLGH, was used for the incorporation of drugs such as NO-releasing materials, while maintaining the characteristics of PLGA.³³⁻³⁵

Delivery of the gasotransmitters, however, requires overcoming some drawbacks, including their short half-life, stability, the solubility of the donors, and ensuring a controlled release without an initial burst. NO release from the polymer-pendent moieties can facilitate diverse applications,³⁶⁻³⁹ also showing a suppressed release behavior in polymeric particles.^{35,40} Similarly, H₂S-releasing molecules have been

developed to overcome the insoluble issue and initial bursting of H₂S–donating molecules.^{18,41} Both gasotransmitters (NO and H₂S) can be delivered by macromolecules (–conjugating donors or –encapsulation), which leads to appropriate biological functions with “controlled” or “slow” release behaviors. My research group previously reported inducing angiogenesis by the controlled release of NO from the self–assembled nanoparticles by amphiphilic copolymers.²² In this study, I designed self–assembled polymeric nanoparticles for the delivery of nitric oxide and hydrogen sulfide simultaneously (**Fig. 1**). For ensuring the cooperation of the two gasotransmitters (NO and H₂S), I modified methoxy poly (ethylene glycol–*b*–lactic–*co*–glycolic acid) (mPEG–PLGA) with 2,2–bis(hydroxymethyl) propionic acid (HMPA) and 4–aminothiobenzamide for cysteine–triggered H₂S release. The self–assembled nanoparticles were characterized and displayed enhanced angiogenic potential *in vitro* and *ex vivo*.

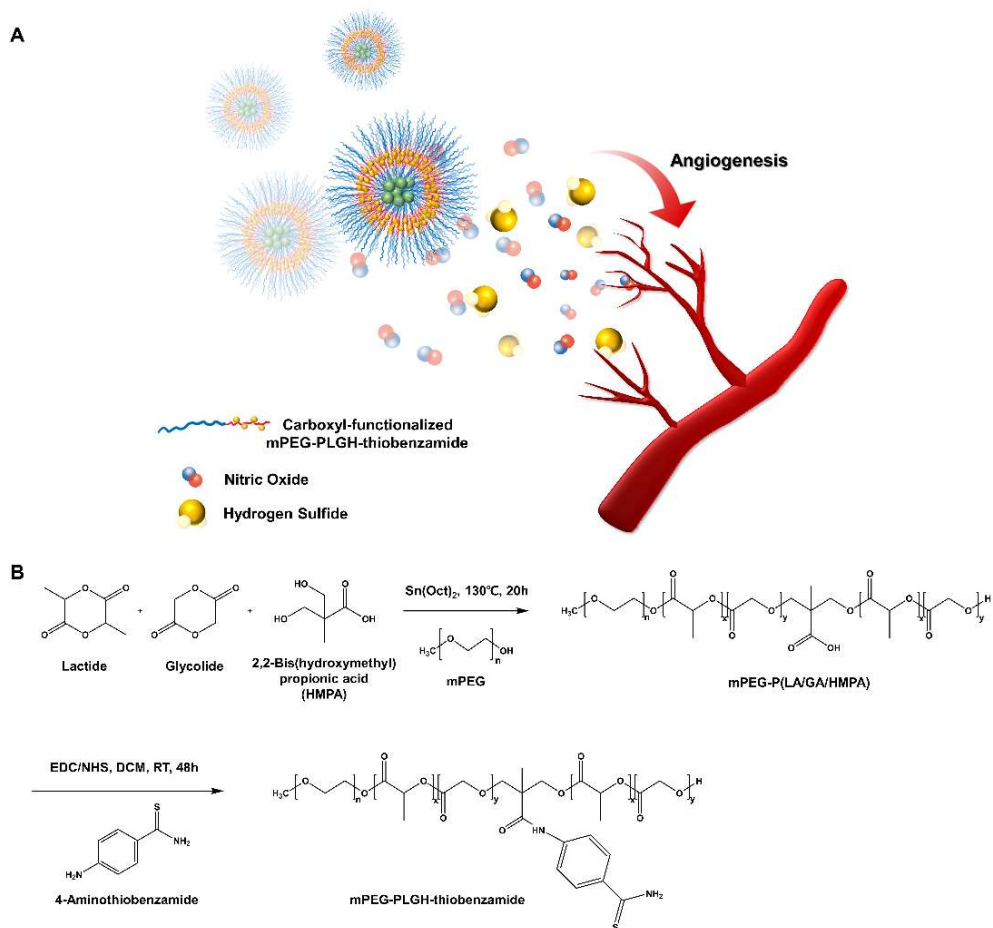


Fig. 1 (A) Schematic illustration of NO & H₂S co-delivery from self-assembled methoxy poly (ethylene glycol-*b*-lactic-*co*-glycolic-*co*-hydroxymethyl propionic acid)-thiobenzamide (mPEG-PLGH-thiobenzamide, PTA) nanoparticles for enhancing angiogenesis. (B) Synthesis scheme of mPEG-PLGH and PTA copolymers.

Chapter 2. Results and discussion

2.1. Characterization of mPEG–PLGH and mPEG–PLGH–thiobenzamide (PTA) copolymers

To deliver two different molecules together, biodegradable amphiphilic mPEG–PLGA–based mPEG–PLGH–thiobenzamide (PTA) copolymers were prepared and characterized by ^1H NMR and FT–IR. First, mPEG–PLGH copolymers, which have carboxylic functional groups in the backbone chain of mPEG–PLGA as H_2S –donor–conjugating moieties, were successfully polymerized by a ring–opening polymerization with L–lactide, glycolide, and HMPA. PTA copolymers were synthesized by conjugating 4–aminothiobenzamide, which acts as a H_2S donor, to the carboxylic moieties with an amide bond. All the peaks of the ^1H NMR spectrum confirmed the PTA copolymer structures (**Fig. 2A**). The peaks at 5.2 and 1.6 ppm were attributed to the methine and methyl proton of the lactic acid repeat units. The methylene protons of mPEG and glycolic acid repeat units were presented at 3.6 and 4.8 ppm, respectively. The methyl and methylene protons of HMPA were revealed at 1.25 and 4.3 ppm. The peak at 2.8 ppm presented hydrogen environments directly

bonded to an aromatic ring.

FT-IR was used for further compositional analysis of the mPEG-PLGH and PTA copolymers (**Fig. 2B**). The strong sharp band at 1750 cm^{-1} was attributed to the carbonyl C=O stretch, and the $1080\text{--}1170\text{ cm}^{-1}$ bands corresponded to the C-O stretch. The peaks at $2875\text{--}2997\text{ cm}^{-1}$ were assigned to the C-H stretch, and the bands at $1386\text{--}1457\text{ cm}^{-1}$ were assigned to the C-H bending vibrations. The peaks at 1630 and 1550 cm^{-1} were attributed to the amide C=O bond and aromatic ring C-C stretch of conjugated thiobenzamide, respectively. The molecular weights of the copolymers were measured by GPC (**Table S1**). According to the GPC results, the conjugation of thiobenzamide to the mPEG-PLGH backbone could be confirmed by the increased M_w of the PTA copolymers in comparison with the mPEG-PLGH copolymers.

2.2. Characterization of PTA-NO-NPs

The polymeric PTA-NO-NPs were successfully prepared by a water-in-oil-in-water (W/O/W) double emulsion with core-shell structures. The PTA-NO-NPs were able to self-assemble into a vesicular form with separated hydrophilic and hydrophobic

regions, because of the amphiphilicity with appropriate volume fractions of the blocks.⁴²⁻⁴⁴ H₂S-releasing 4-aminothiobenzamide was chemically conjugated into the hydrophobic region, while NO-releasing DETA NONOates were physically encapsulated into the hydrophilic core. Several properties that would be considered for useful nanoparticles were characterized, such as the appropriate particle size, entrapment efficiency, and release profile.⁴⁵

The prepared PTA-NO-NPs were well distributed with an average size of 140.8 ± 4.0 nm (**Fig. 2C**), indicating that the PTA-NO-NPs had a suitable size as a nano-based delivery system to sustain a longer circulation.^{22,46} The zeta potential, one of the critical characteristics of nanoparticles, was also estimated by DLS. The PTA-NO-NPs had an average zeta potential of -1.87 ± 0.36 mV, which is a slightly more negative charge than that exhibited generally in PLGA-based nanoparticles (**Fig. 2D**).

TEM images confirmed the morphology of the PTA-NO-NPs (**Fig. 2E**). The image of PTA-NO-NPs presented clear spherical core-shell structures resulting from the double-emulsion method of fabrication of amphiphilic PTA copolymers. The results indicated that the PTA-NO-NPs were uniformly made in a size of about 140 nm according to the DLS results. The

entrapment efficiency is an important property to evaluate the drug-loading ability of nanoparticles. The entrapment efficiency of DETA NONOates measured from hydrolyzed PTA-NO-NPs was $53.7 \pm 4.1\%$ (data not shown), which was much higher than for previously reported PLGA-based particles prepared in the same W/O/W method.⁴⁷

2.3. Release measurement of NO and H₂S

The release behaviors of NO and H₂S from the nanoparticles were confirmed respectively in physiological conditions. Using the Griess assay, which is generally used for measuring NO concentration by detecting nitrite or nitrate oxidized from NO, NO release from the PTA-NO-NPs was confirmed (**Fig. 2F**). At a concentration of 1 mg mL^{-1} , PTA-NO-NPs encapsulating DETA NONOates exhibited a sustained NO-release profile for 72 h of up to approximately 20 nmol. As already revealed, free DETA NONOates have issues with an initial NO burst release generating two NO products. However, the PTA-NO-NPs released NO in a controlled manner similar to in the previous study.²²

H₂S release from the PTA-NO-NPs was assessed by the

methylene blue method, which is commonly used to monitor the H₂S concentration by colorimetric measurement. The H₂S release test proceeded with 4 mM of L-cysteine as a thiobenzamide-trigger agent, because arylthioamides releases H₂S in the presence of organic thiols, such as reduced glutathione, L-cysteine.^{48,49} The H₂S release also showed a long-lasting sustained-release profile (**Fig. 2G**). The H₂S release from PTA-NO-NPs at 1 mg mL⁻¹ was controlled with a low concentration under the range of 15 μM. After 12 h, a constantly increasing behavior in H₂S concentration was observed over 72 h. Even though H₂S accumulated continuously over time, PTA-NO-NPs were expected not to affect biocompatibility because of their very low concentration. Many previous studies have reported that arylthioamides can cause several issues, such as (1) toxicity caused by high concentration, (2) uncontrolled release mechanisms, (3) stability of prodrugs.⁵⁰ Whereas, my PTA-NO-NPs showed the potential to overcome these problems by delivering in nanoparticles.

A controlled release profile in a drug-delivery system can increase the drug bioavailability with a prolonged circulation time and can decrease the side effects from burst drug release. For inducing angiogenesis effectively, NO and H₂S should be released

at low concentration and for a long time. Compared to compounds such as NOSH–aspirin and ZYZ–803, which bear NO– and H₂S–releasing materials together and have a release time of about 2 h, the PTA–NO–NPs showed a prolonged release and increased circulation time of about 3 days.²⁵ This release behavior is assumed to be caused via diffusion or degradation of the core–shell structured nanoparticles. Because of the slow and prolonged release profile, its application could be variable by adjusting the concentration of the PTA–NO–NPs.

| | M_n | M_w | PDI |
|--------------------------------|----------------------|----------------------|-------------|
| mPEG-PLGH | 10186 | 12732 | 1.25 |
| mPEG-PLGH-thiobenzamide | 12503 | 16114 | 1.28 |

Table. S1 Molecular weight of mPEG–PLGH and PTA copolymers. Determined by GPC using DMF as eluent. The data are displayed as the mean \pm SEM (n = 5). (M_n: number average of molecular weight, M_w: weight average of molecular weight, PDI: polydispersity index; M_w/M_n)

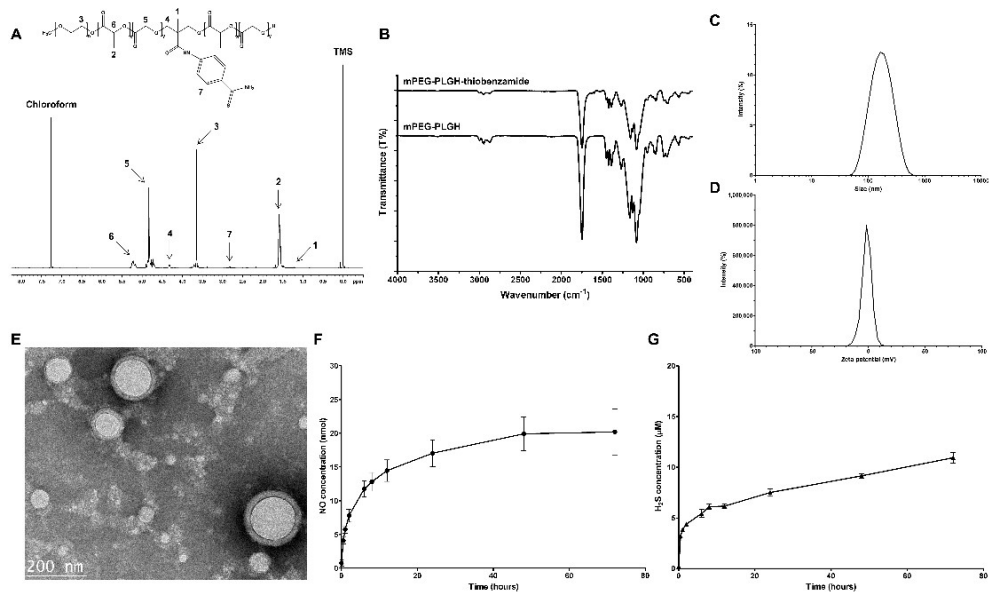


Fig. 2 Characterization of the PTA copolymers and PTA-NO-NPs. (A) ¹H NMR spectrum of the PTA copolymers with D-chloroform as a solvent. (B) FT-IR spectra of the mPEG-PLGH and PTA copolymers. (C) Size distribution and (D) zeta potential confirmed by DLS. The data are displayed as the mean \pm SEM (n = 4). (E) Morphological analysis was determined by TEM. The scale bar is 200 nm. (F) Nitric oxide release measurement by Griess assay and (G) Hydrogen sulfide release measurement by the methylene blue method were carried out *in vitro*. PTA-NO-NPs at 1 mg ml⁻¹ were tested under physiological conditions. The data are displayed as the mean \pm SEM (n = 3).

2.4. *In vitro* cytotoxicity of PTA–NO–NPs

To evaluate the cytotoxicity of the PTA–NO–NPs for physiological use, *in vitro* CCK–8 and LIVE/DEAD assays were carried out with HUVECs, 3T3–L1, A549, C6, MCF–7, and ADSC cell lines. The cytotoxicity tests were performed with three different concentrations (50, 100 $\mu\text{g mL}^{-1}$, and 1 mg mL^{-1}), which were determined based on the results from the NO– and H₂S–release tests. Quantitative analysis was carried out by CCK–8 assay (**Fig. 3A** and **S1**). For all the cell types, the PTA–NO–NPs at 50 and 100 $\mu\text{g mL}^{-1}$ concentration showed high cell viabilities compared to the control group at every time point, with the cell viabilities mostly above 100%. On the other hand, PTA–NO–NPs at 1 mg mL^{-1} , which represents a relatively high concentration, showed toxicity to all cell types. Especially in the 3T3–L1 and C6 cell lines, the toxicity of PTA–NO–NPs was conspicuously high, with under about 60% cell viabilities after 24 h.

Fluorescence images were obtained by the Live/Dead assay to further assess the cytotoxicity of the PTA–NO–NPs. The results were matched to those of the CCK–8 assay (**Fig. 3B** and **S2**). PTA–NO–NPs at 50 and 100 $\mu\text{g mL}^{-1}$ showed a high

living-cell density and few dead cells, similar to the control group in all cell types at all time points; whereas a relatively high concentration of PTA-NO-NPs (1 mg mL^{-1}) showed a low living-cell density and increased red fluorescence in comparison to the control at 50 and $100 \text{ } \mu\text{g mL}^{-1}$, which means that a large number of cells were dead and detached by the cytotoxicity of high NO and H₂S concentrations.

Various concentrations of PTA-NO-NPs and cell types were examined to observe the influence of PTA-NO-NPs on the reported physiological functions induced by NO and H₂S in addition to confirm the biocompatibility. As reported previously, a low concentration of NO or H₂S mediates cell proliferation and vascular effects, while a high concentration induces cell apoptosis. From that point of view, 50 and $100 \text{ } \mu\text{g mL}^{-1}$ were selected for the low NO and H₂S concentration groups with biocompatibility and 1 mg mL^{-1} was selected for the high concentration group with cytotoxicity. 3T3-L1 was assessed because the fibroblast is the most common type of cell discovered in connective tissue, and HUVECs were observed because the endothelial cells are substantially involved in angiogenesis. Also, because NO and H₂S are known to play an important role in cancer progress and therapy,^{1,51} various cancer

cell lines, including C6 (mouse brain glial cell), A549 (lung carcinoma), and MCF-7 (breast adenocarcinoma), were assessed. ADSCs, which are stem cells that can differentiate into many different cell types, were tested to observe the proliferation ability of the PTA-NO-NPs.

From the results, the PTA-NO-NPs at low concentration were demonstrated to be biocompatible and showed potent cell proliferation and angiogenesis. On the other hand, the PTA-NO-NPs at high concentration were highly effective at inducing apoptosis in a dose-dependent manner, and therefore could be promising anticancer therapeutic materials. Thus, my nanoparticles were verified to have various physiological functions that mean they could serve as a multifunctional therapeutic material in a wide range of clinical applications in the future.

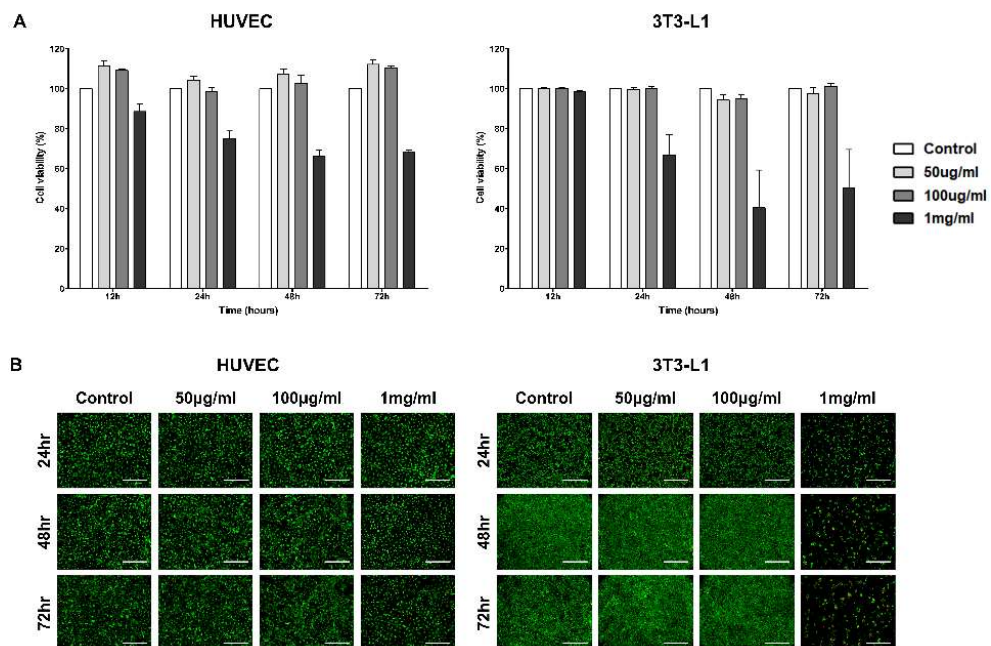


Fig. 3 *In vitro* cytotoxicity measurement of HUVECs and 3T3-L1. (A) Quantitative cytotoxicity analysis was proceeded by the CCK-8 assay. The data are displayed as the mean \pm SEM (n = 4). (B) Fluorescence images of cells obtained by Live/Dead assay. Green channel represents live cells and red channel represents dead cells (scale bar = 500 μ m).

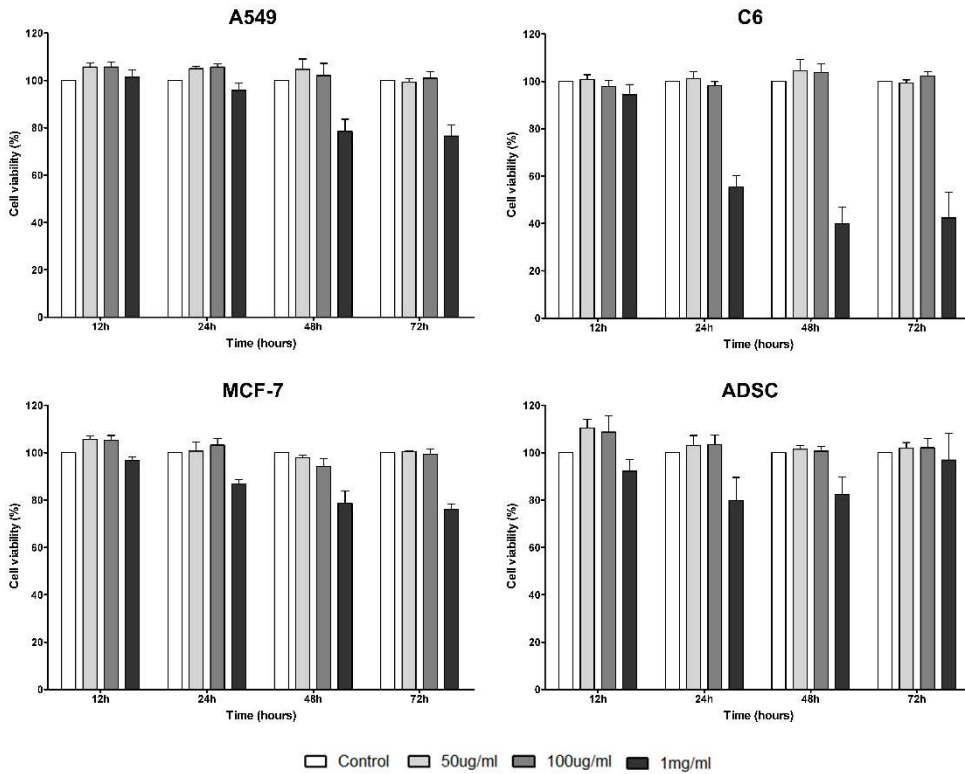


Figure. S1 *In vitro* cytotoxicity measurement by CCK-8 assay. Cancer cell lines (A549, C6, MCF-7) and ADSCs were tested. The data are displayed as the mean \pm SEM (n = 4).

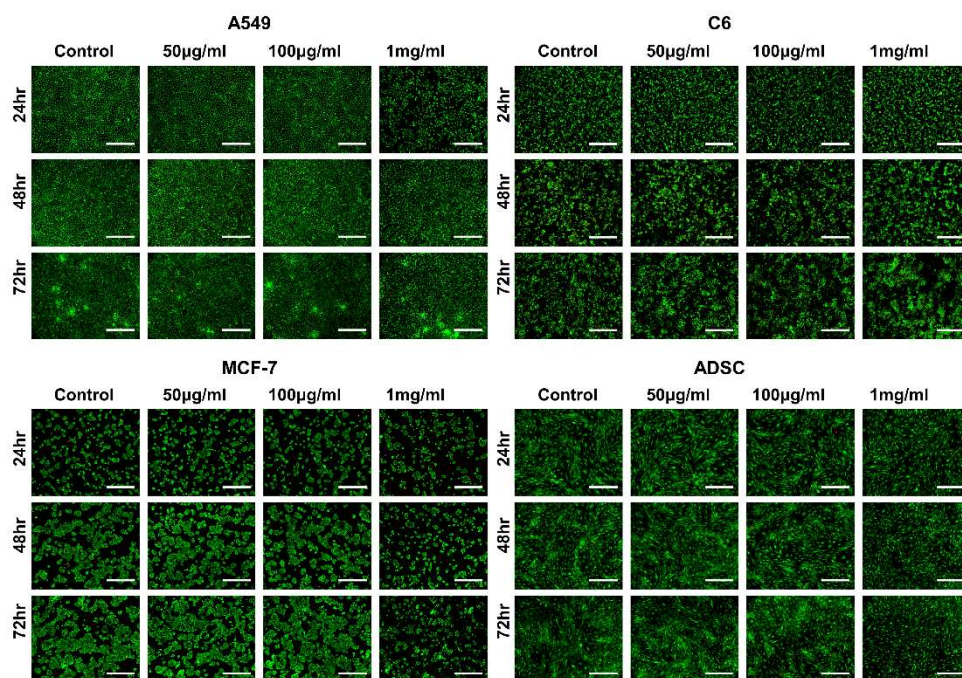


Figure. S2 Fluorescence images of cells were obtained by Live/Dead assay. Cancer cell lines (A549, C6, MCF-7) and ADSCs were tested. Green channel represents live cells and red channel represents dead cells. (Scale bar = 500 μ m)

2.5. Angiogenic potential of the PTA–NO–NPs

The angiogenic property of the PTA–NO–NPs was assessed by an *in vitro* tube assay and *ex vivo* aortic ring assay. To demonstrate the synergistic angiogenic ability by co-delivery of NO and H₂S from PTA–NO–NPs, DETA NONOates as a NO donor only group and PTA–NPs as a H₂S donor only group were also tested. First, a tube formation assay was performed *in vitro*, and the tubular branching ability by HUVECs was assessed (**Fig. 4**). PTA–NO–NPs at various concentration were tested, and the results showed that all the groups treated with PTA–NO–NPs had much higher angiogenic potentials than the negative control group. Moreover, HUVECs treated with PTA–NO–NPs formed more tubes in comparison to the group treated with VEGF. Besides, PTA–NO–NPs at 10, 25, and 50 $\mu\text{g mL}^{-1}$ induced more tubes than DETA NONOates and PTA–NPs with statistically significant differences ($p < 0.001$ for 10 and 25 $\mu\text{g mL}^{-1}$, $p < 0.01$ for 50 $\mu\text{g mL}^{-1}$; data not shown). Below 25 $\mu\text{g mL}^{-1}$, the number of tube branches was increased in proportion to the PTA–NO–NP concentration. At 25 $\mu\text{g mL}^{-1}$, tubes were formed the most, and above that tube branches were decreased gradually.

Furthermore, the aortic ring assay was performed using rat aorta for an *ex vivo* study. This assay is an organ culture-based model that can be used to observe the ability to sprout new microvessels from aorta. I observed enhanced angiogenic potentials in PTA-NO-NPs (10 and 25 $\mu\text{g mL}^{-1}$) at day 7. The area of sprouted neovessels was evaluated. Since a higher angiogenic potential can induce more microvessel sprouting, the outgrowth area of neovessels would be a marker of angiogenic estimation. The results were comparable to the results of my *in vitro* study (**Fig. 5**). In all groups treated with PTA-NO-NPs, new microvessels sprouted more than the groups of EBM2 and EBM2 with VEGF. Also, the angiogenic potentials were slightly increased in the PTA-NO-NP groups compared to the DETA NONOates and PTA-NPs groups. Between 10 and 25 $\mu\text{g mL}^{-1}$, there were no significant differences in the microvessel sprouting abilities of the PTA-NO-NPs.

The results showed that only NO or H₂S groups could promote angiogenesis rather than the control group and VEGF treated group, whereas PTA-NO-NPs induced angiogenesis more strongly. This means that NO and H₂S can induce angiogenesis independently, but the angiogenic potential was much higher when delivering NO and H₂S together in nanoparticles than in

delivering each separately. Despite the low release concentration of H₂S from PTA-NO-NPs, the results exhibited that the released H₂S can fully help NO signal amplification. Because of the much longer release time than delivery by the compounds, the delivery of NO and H₂S by PTA-NO-NPs is expected to be more effective in angiogenesis.

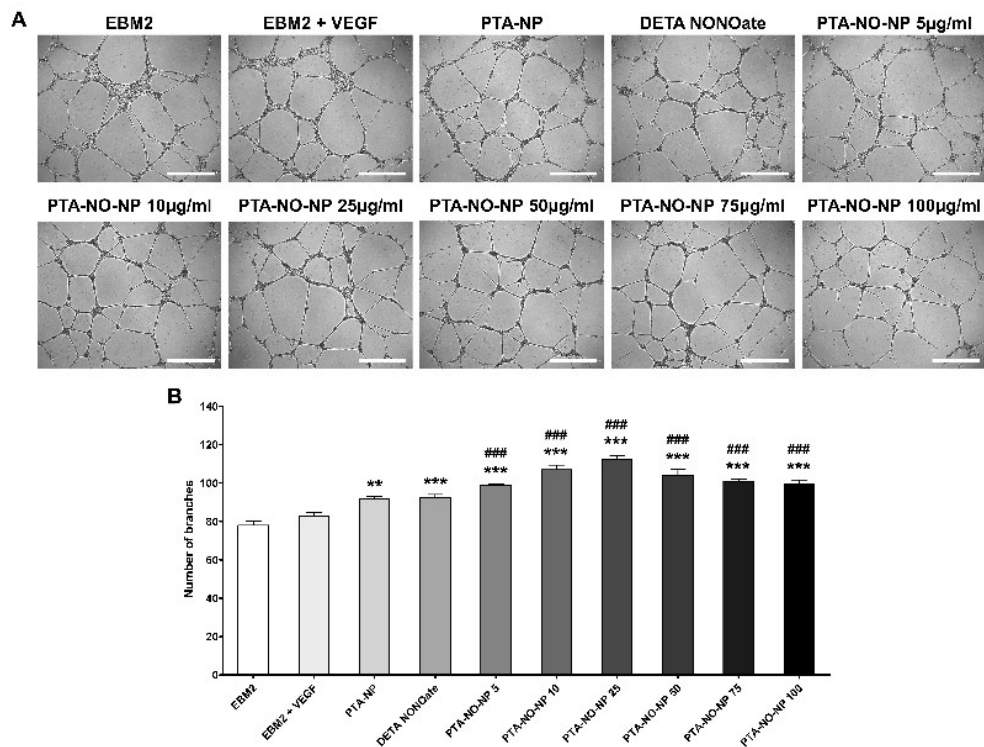


Fig. 4 Endothelial cell tube formation assay to assess the angiogenic potential of PTA-NO-NPs *in vitro*. Data are shown for HUVECs on a matrigel matrix at 16 h. (A) Representative microscopic images (scale bar = 500 μ m). (B) The average number of tube branches formed in the assay was measured. The data are displayed as the mean \pm SEM (n = 4). Statistical differences between the experimental groups were determined using oneway ANOVA test followed by Tukey' s test (** p < 0.001 vs. EBM2, ### p < 0.001 vs. EBM2 + VEGF).

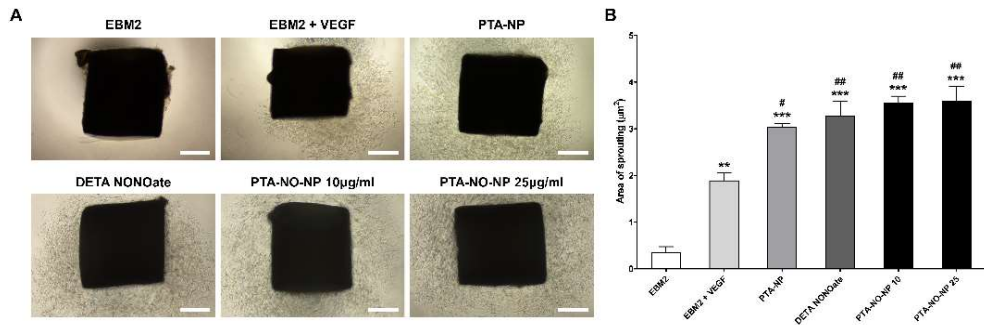


Fig. 5 *Ex vivo* aortic ring assay using rat aorta. (A) Representative microscopic images of sprouted microvessels from the aorta after 7 days of incubation (scale bar = 500 μ m). (B) The area of new microvessels outgrowth was quantified by ImageJ software. The data are displayed as the mean \pm SEM (n = 3). Statistical differences between experimental groups were determined using one-way ANOVA test followed by Tukey's test (** p < 0.001 vs. EBM2, ### p < 0.001 vs. EBM2 + VEGF).

Chapter 3. Experimental

3.1. Materials

Lactic acid, glycolic acid, HMPA (2,2-bis(hydroxymethyl)propionic acid), and stannous octoate were supplied by Sigma Aldrich (St Louis, MO, USA). Methoxy poly (ethylene glycol) (mPEG) (average Mw 2000) was supplied by Tokyo Chemical Industry (Tokyo, Japan). 4-Aminothiobenzamide was purchased from Carbosynth (Berkshire, UK) and diethylenetriamine NONOate (DETA NONOate) was supplied by Acros Organics. The nitric oxide assay kit was purchased from Abcam (Cambridge, UK). The dialysis membrane (Spectra/por 6 MWCO 1 kDa) was purchased from Spectrum Industries, Inc. (Los Angeles, CA, USA). 3T3-L1 (mouse fibroblast), C6 (mouse brain glial cell), A549 (lung carcinoma), and MCF-7 (breast adenocarcinoma) cell lines were obtained from Korea Cell Line Bank (Seoul, Korea). HUVECs (human umbilical vein endothelial cell) and ADSC (adipose-derived stem cell) cell lines were supplied by PromoCell (Heidelberg, Germany) and Cefo Co., Ltd (Seoul, Korea), respectively. The Cell Counting Kit-8 (CCK-8) was supplied by Dojindo Molecular Technologies (Rockville, MD,

USA) and the LIVE/DEAD Viability/Cytotoxicity kit was supplied by Thermo Fisher Scientific (Waltham, MA, USA).

3.2. Preparation of mPEG–PLGH copolymers (carboxyl–functionalized mPEG–PLGA)

mPEG–PLGH copolymers were polymerized through a typical ring–opening polymerization using stannous octoate catalyst, as reported previously.^{22,52} Briefly, lactide (4 mmol), glycolide (4 mmol), HMPA (0.09 mmol), and mPEG (20 wt% of the total monomer) were added into a flask, and the flask was sealed. After the flask was immersed in an oil bath, stannous octoate (0.1 wt% of the total monomer) was added as a catalyst. For 20 h, the mixture was gently stirred at 130 °C in an N₂ environment. After quenching the polymerization by cooling down, the crude product was dissolved in DCM and precipitated out by adding excess methyl alcohol. The product was washed with methyl alcohol and then recovered by drying under vacuum for 24 h at room temperature.

3.3. Preparation of mPEG–PLGH–thiobenzamide (PTA) copolymers

mPEG–PLGH–thiobenzamide (PTA) copolymers were prepared by conjugating 4–aminothiobenzamide to the carboxyl residue of mPEG–PLGH copolymers with an amide bond, as described previously.^{33,35} The carboxyl–functionalized mPEG–PLGH and NHS (2.5 molar eq. to carboxyl group) were mixed in DMF (4 vol.) in an N₂ environment. After EDC · HCl (2.5 molar eq.) was dissolved in DMF (6 vol.), the solution was added into the mixture. The synthesis was proceeded at room temperature for 24 h to activate all the available carboxyl groups of mPEG–PLGH. 4–Aminothiobenzamide (5 molar eq.) solution mixed with triethylamine (8 molar eq.) in DMF (2 vol.) was added into the activated mPEG–PLGH copolymer mixture in an N₂ environment and maintained with stirring gently for 24 h at room temperature. The resulting solution was concentrated to remove DMF, and then the crude residue was precipitated using excess diethyl ether. The precipitate was redissolved in DCM and extracted two times with saturated NaCl solution to remove any remaining salts and excess 4–aminothiobenzamide. The clear DCM phase was separated, and then the solvent was removed by distillation.

After recrystallization using excess cold diethyl ether, the product was obtained using a vacuum oven at room temperature for 24 h.

3.4. Preparation of PTA nanoparticles with DETA NONOate (PTA-NO-NPs)

PTA-NO-NPs encapsulating DETA NONOate were prepared through the previously reported water-in-oil-in-water (W/O/W) double emulsion method.^{22,53} Briefly, 20 mg of PTA was dissolved in 1 mL of DCM, and then 0.2 mL of DW (for PTA-NPs) or 5 wt% DETA NONOate solution (in 10 mM NaOH) was mixed. Using a probe sonicator, the mixture was emulsified for 3 min in an ice bath. Next, 2 mL of 2% polyvinyl alcohol in DW was added into the emulsion, followed by emulsification by sonication for 5 min. The final emulsion was mixed with 15 mL of 0.2% polyvinyl alcohol solution and filtered with a 0.45 μ m PES syringe filter. After the solution was diluted with DW, the final PTA-NO-NPs or PTA-NPs were freeze-dried for at least 3 days and then collected.

3.5. Characterization of the mPEG–PLGH and PTA copolymers

To verify the PTA copolymer structure, ^1H nuclear magnetic resonance spectrometry (^1H NMR, ADVANCE II 500, Bruker, Billerica, MA, USA) was used with d-chloroform as a solvent. To confirm the structures of mPEG–PLGH and PTA copolymers, Fourier transform infrared spectrometry (FT–IR, Bruker Corporation, Billerica, MA, USA) was used. To assess the molecular weight of the copolymers, gel permeation chromatography (GPC, Ultimate 3000, Thermo Fisher Scientific, Waltham, MA, USA) was used with DMF as a solvent.

3.6. Characterization of the size distribution and morphology of the PTA–NO–NPs

A zetasizer instrument (Malvern Instruments, Malvern, UK) was used to assess the size distribution and zeta potential of the PTA–NO–NPs. The measurement was carried out with a 173° scattering angle at room temperature with the PTA–NO–NPs well-dispersed in DW. For morphological characterization, field emission transmission electron microscopy (FE–TEM, JEM–

F200, JEOL Ltd, Tokyo, Japan) was used. To pretreat the PTA–NO–NPs, negative staining was conducted using sodium phosphotungstate solution (1%).

3.7. Entrapment efficiency measurement of the PTA–NO–NPs

The DETA NONOate entrapment efficiency of the PTA–NO–NPs was measured as previously described using a Nanodrop 2000 spectrophotometer (Thermo Fisher Scientific, Waltham, MA, USA).⁵⁴ The PTA–NO–NPs dispersed in NaOH (1 M) were kept under ultrasonication for at least 10 min, and then continuously stirred for complete hydrolysis of the PTA–NO–NPs. The absorbance of the completely decomposed PTA–NO–NP mixture was measured at 252 nm wavelength. The standard solution of PTA–NPs and an equivalent amount of DETA NONOate were prepared in 1 M NaOH for carrying out the calibration. The DETA NONOate entrapment efficiency was determined using the equation as follows:

$$\text{Entrapment efficiency (\%)} = \frac{\text{Amount of remaining DETA NONOate in the NPs}}{\text{Amount of initially added DETA NONOate}} \times 100$$

3.8. NO–release measurements

To confirm the NO release from the PTA–NO–NPs, the Griess assay was performed with a nitric oxide assay kit following the manufacturer's protocol. The Griess assay is a common analytical test that measures the presence of nitrite and nitrate. DETA NONOate can spontaneously dissociate and release two NO products under normal physiological conditions. Briefly, PTA–NO–NPs (2 mg) encapsulating DETA NONOate were fully dispersed in PBS (2 mL). The dispersed solution was placed into a dialysis membrane, so that NO can be diffused freely across the membrane. Then, the dialysis membrane was immersed in 6 mL of PBS and incubated at 37 °C in darkness. Next, 85 μ L of sample was taken at each time point, and after that nitrate reductase (5 μ L) and enzyme cofactor (5 μ L) were added. Each sample was incubated at room temperature for 1 h to convert nitrate to nitrite by nitrate reductase. Enhancer (5 μ L) was added into each sample, and then incubated for 10 min at room temperature. After the Griess reagents were mixed, the optical density was measured by a microplate reader (Synergy H1, Bio Tek, Winooski, VT, USA) at 540 nm. The total amount of NO, which is the sum of nitrate and nitrite, was calculated

against a standard curve.

3.9. H₂S–release measurements

H₂S release from the PTA–NO–NPs was confirmed by using the methylene blue method as previously reported.⁴⁸ The methylene blue method is a colorimetric assay for measuring the intensity of methylene blue color directly proportional to the H₂S concentration. In the presence of L–cysteine, arylthioamides can produce H₂S. Briefly, 0.5 mL of L–cysteine in PBS (4 mM) was added into 0.1 mL of zinc acetate in DW (1% w/v). After 0.5 mL of PTA–NO–NPs (1 mg mL⁻¹) in DW was mixed, the mixture was incubated at 37 °C in darkness. At each time point, 150 μL of 20 mM N,N–dimethyl–p–phenylenediamine dihydrochloride dye in 7.2 M HCl and 150 μL of 30 mM iron (III) chloride in 1.2 M HCl were added into the samples, which resulted in the formation of methylene blue. After 10 min, the H₂S concentration of each sample was measured by a microplate reader at 670 nm and calculated against a calibration curve. NaHS, a representative H₂S–releasing molecule, was used to graph the standard curve of H₂S release. PBS (0.5 mL) was mixed with zinc acetate (0.1 mL) followed by adding 0.5 mL of NaHS in DW (0–300 μM).

The samples were incubated for 30 min under the same conditions described above for the trapping of H₂S by zinc acetate and for transforming into stable zinc sulfide. Then the samples were mixed with N,N-dimethyl-p-phenylenediamine dihydrochloride dye and iron (III) chloride and measured at 670 nm as described above.

3.10. *In vitro* cytotoxicity measurements

In vitro cytotoxicity was confirmed with 3T3-L1, HUVECs, A549, C6, MCF-7, and ADSC. 3T3-L1 and ADSC were cultured in DMEM containing 10% fetal bovine serum (FBS) and 1% penicillin-streptomycin (PS). A549, C6, and MCF-7 were cultured in RPMI with FBS (10%) and PS (1%). The culture medium for HUVECs was endothelial growth medium-2 (PromoCell, Heidelberg, Germany) with FBS (10 mL), ascorbic acid (0.5 mg), heparin (11.25 mg), human recombinant epidermal growth factor (2.5 μ g), human recombinant basic fibroblast growth factor (5 μ g), hydrocortisone (0.1 mg), insulin-like growth factor (R3 IGF-1) (0.01 mg), and human recombinant vascular endothelial growth factor 165 (0.25 μ g). For the CCK-8 assay, 1×10^4 cells of each cell line were incubated in 96 well

plates at 37 °C treated with PTA–NO–NPs in the concentration of 50, 100 $\mu\text{g mL}^{-1}$, or 1 mg mL^{-1} . At 12, 24, 48, and 72 h, the cytotoxicity was determined at 450 nm using the microplate reader. For the Live/Dead assay, the cells were placed in 48 well plates in the same conditions as described above. At 24, 48, and 72 h, the fluorescence images were randomly obtained by fluorescence microscopy (Axio Observer Z1, Carl Zeiss, Oberkochen, Germany).

3.11. Tube formation assay

To verify the angiogenic potential of the PTA–NO–NPs *in vitro*, a tube formation assay was performed. The tube formation assay is a commonly used method to measure the ability of formation of new blood vessels by endothelial cells in a quantifiable manner.⁵⁵ Growth factor reduced matrigel (Corning Incorporated, New York, NY, USA) was evenly distributed to each well as the basement membrane matrix. The coated well plate was incubated at room temperature for 30 min and under humidified conditions (5% CO_2 , 37 °C) for 1 h. The prepared conditioned media was added to each well in a two-fold concentration. As the control medium, the endothelial cell growth

basal medium-2 (EBM2, Lonza, Basel, Switzerland) with FBS (10 mL) and gentamicin-amphotericin (0.5 mL) and without any other growth factors was prepared. EBM2 with 0.1% (v/v) VEGF was prepared to compare the angiogenic potential of the PTA-NO-NPs against VEGF. Also, the media containing PTA-NPs (25 $\mu\text{g mL}^{-1}$), DETA NONOate (1.7 $\mu\text{g mL}^{-1}$, the same concentration of DETA NONOate in 25 $\mu\text{g mL}^{-1}$ PTA-NO-NPs), and PTA-NO-NPs (5, 10, 25, 50, 75, and 100 $\mu\text{g mL}^{-1}$) were prepared for the test media. The media-treated well plate was incubated under humidified 37 °C, 5% CO₂ conditions for 1 h. Among the endothelial cell lines, HUVECs were prepared and transferred into each well. After incubation for 16 h, the tubular network was imaged by a microscope and the number of tubular branches was counted using ImageJ.

3.12. Aortic ring assay

To further assess the angiogenic properties in an *ex vivo* model, a rat aorta ring assay was performed.⁵⁶ Animal experiments were performed with the approval (Approval No. BA-1903-268-017-01) of the Institute of Animal Care and Use Committee of Seoul National University Bundang Hospital.

First, matrigel matrix was used to precoat each well and incubated under 5% CO₂ and 37 °C conditions for 30 min. Rat aortas (4-week-old female Sprague Dawley rats; Orient, Seongnam, Korea) were excised and sliced into rings in 1.5 mm widths. Every single ring was located in the top center of each well, followed by incubation for 10 min. On top of each ring, supplemental matrigel matrix was added. After incubation for 30 min, EBM2, EBM2 with VEGF, PTA-NPs (25 μg mL⁻¹), DETA NONOate (1.7 μg mL⁻¹), and PTA-NO-NPs (10 and 25 μg mL⁻¹) were added to each well. The well plate was incubated under 37 °C, 5% CO₂ conditions and all the conditioned media were changed at day 3. After 7 days, sprouting microvessels were imaged using a microscope and the area of sprouting was calculated using ImageJ.

3.13. Statistical analysis

All the results are represented as the mean ± SEM of independent experiments. The significance of statistical differences was analyzed using one-way ANOVA test (Prism; GraphPad Software, San Diego, CA, USA). $P < 0.05$ was regarded to have statistical significance.

Chapter 4. Conclusions

In this study, PTA-NO-NPs releasing NO and H₂S together were prepared by a double emulsion from amphiphilic PTA copolymers. I demonstrated the synergistic effect of the co-delivery of two gas molecules, NO and H₂S, via nanoparticles for enhancing angiogenesis. In contrast with compounds bearing NO- and H₂S-releasing moieties, the PTA-NO-NPs exhibited controlled NO- and H₂S-release profiles with a prolonged circulation time. With this sustained-release manner, PTA-NO-NPs at low concentration showed biocompatibility. Furthermore, through the *in vitro* and *ex vivo* assays, I confirmed the enhanced angiogenic effect caused by the co-delivery of NO and H₂S from PTA-NO-NPs compared to the groups delivering each gas molecule separately. To the best of my knowledge, this study is the first application of NO and H₂S into nano-sized delivery vehicles for the purpose of inducing angiogenesis. I believe that my PTA-NO-NPs have potential as an effective delivery system for inducing angiogenesis and other various physiological functions that are affected by both NO and H₂S.

References

1. C. Yang, S. Jeong, S. Ku, K. Lee and M. H. Park, *J. Controlled Release*, 2018, 279, 157—170.
2. R. Wang, *Trends Biochem. Sci.*, 2014, 39, 227—232.
3. A. K. Mustafa, M. M. Gadalla and S. H. Snyder, *Sci. Signal.*, 2009, 2, re2.
4. H. Kimura and H. Esumi, *Acta Biochim. Pol.*, 2003, 50, 49—59.
5. X. Cao, L. Ding, Z. Xie, Y. Yang, M. Whiteman, P. K. Moore and J. Bian, *Antioxid. Redox Signaling*, 2019, 31, 1—38.
6. E. A. Wintner, T. L. Deckwerth, W. Langston, A. Bengtsson, D. Leviten, P. Hill, M. A. Insko, R. Dumpit, E. V. Ekart, C. F. Toombs and C. Szabo, *Br. J. Pharmacol.*, 2010, 160, 941—957.
7. M. Magierowski, K. Magierowska, S. Kwiecien and T. Brzozowski, *Molecules*, 2015, 20, 9099—9123.
8. S. Yuan, X. Shen and C. G. Kevil, *Antioxid. Redox Signaling*, 2017, 27, 634—653.
9. S. C. Bir, C. B. Pattillo, S. Pardue, G. K. Kolluru, X. Shen, T. Giordano and C. G. Kevil, *J. Am. Heart Assoc.*, 2014, 1, e004093.

10. S. H. Francis, J. L. Busch, J. D. Corbin and D. Sibley, *Pharmacol. Rev.*, 2010, 62, 525—563.
11. C. Coletta, A. Papapetropoulos, K. Erdelyi, G. Olah, K. Módis, P. Panopoulos, A. Asimakopoulou, D. Gerö, I. Sharina, E. Martin and C. Szabo, *Proc. Natl. Acad. Sci. U. S. A.*, 2012, 109, 9161.
12. D. J. Polhemus and D. J. Lefer, *Circ. Res.*, 2014, 114, 730—737.
13. Y. Qian and J. B. Matson, *Adv. Drug Delivery Rev.*, 2017, 110—111, 137—156.
14. K. M. Dillon, R. J. Carrazzone, J. B. Matson and K. Kashfi, *Biochem. Pharmacol.*, 2020, 176, 113931.
15. A. B. Seabra and N. Durán, *J. Mater. Chem.*, 2010, 20, 1624—1637.
16. F. Rong, Y. Tang, T. Wang, T. Feng, J. Song, P. Li and W. Huang, *Antioxidants*, 2019, 8, 556.
17. C.-t. Yang, L. Chen, S. Xu, J. J. Day, X. Li and M. Xian, *Front. Pharmacol.*, 2017, 8, 664.
18. K. Kaur, R. J. Carrazzone and J. B. Matson, *Antioxid. Redox Signaling*, 2019, 32, 79—95.
19. C. R. Powell, K. M. Dillon and J. B. Matson, *Biochem. Pharmacol.*, 2018, 149, 110—123.
20. L. K. Keefer, *ACS Chem. Biol.*, 2011, 6, 1147—1155.

- 21.K. Troidl, S. Tribulova, W.–J. Cai, I. Rüdinger, H. Apfelbeck, W. Schierling, C. Troidl, T. Schmitz–Rixen and W. Schaper, *J. Cardiovasc. Pharmacol.*, 2010, 55, 153–160.
- 22.C. Yang, H. H. Hwang, S. Jeong, D. Seo, Y. Jeong, D. Y. Lee and K. Lee, *Int. J. Nanomed.*, 2018, 13, 6517–6530.
- 23.Y. Zhao, T. D. Biggs and M. Xian, *Chem. Commun.*, 2014, 50, 11788–11805.
- 24.A. Martelli, L. Testai, V. Citi, A. Marino, I. Pugliesi, E. Barresi, G. Nesi, S. Rapposelli, S. Taliani, F. Da Settimo, M. C. Breschi and V. Calderone, *ACS Med. Chem. Lett.*, 2013, 4, 904–908.
- 25.R. Kodela, M. Chattopadhyay and K. Kashfi, *ACS Med. Chem. Lett.*, 2012, 3, 257–262.
- 26.Q. Hu, D. Wu, F. Ma, S. Yang, B. Tan, H. Xin, X. Gu, X. Chen, S. Chen, Y. Mao and Y. Z. Zhu, *Antioxid. Redox Signal.*, 2016, 25, 498–514.
- 27.Y. Lu, D. L. Slomberg and M. H. Schoenfisch, *Biomaterials*, 2014, 35, 1716–1724.
- 28.F. S. Schanuel, K. S. R. Santos, A. Monte–Alto–Costa and M. G. de Oliveira, *Colloids Surf., B*, 2015, 130, 182–191.

- 29.A. Longchamp, K. Kaur, D. Macabrey, C. Dubuis, J.–M. Corpataux, S. Déglise, J. B. Matson and F. Allagnat, *Acta Biomater.*, 2019, 97, 374–384.
- 30.C. Martins, F. Sousa, F. Araújo and B. Sarmiento, *Adv. Healthcare Mater.*, 2018, 7, 1701035.
- 31.J. Cheng, B. A. Teply, I. Sherifi, J. Sung, G. Luther, F. X. Gu, E. Levy–Nissenbaum, A. F. Radovic–Moreno, R. Langer and O. C. Farokhzad, *Biomaterials*, 2007, 28, 869–876.
- 32.J. Yu, A. R. Lee, W. H. Lin, C. W. Lin, Y. K. Wu and W. B. Tsai, *Tissue Eng., Part A*, 2014, 20, 1896–1907.
- 33.V. B. Damodaran, J. M. Joslin, K. A. Wold, S. M. Lantvita and M. M. Reynolds, *J. Mater. Chem.*, 2012, 22, 5990.
- 34.K. A. Wold, V. B. Damodaran, L. A. Suazo, R. A. Bowen and M. M. Reynolds, *ACS Appl. Mater. Interfaces*, 2012, 4, 3022–3030.
- 35.V. B. Damodaran and M. M. Reynolds, *J. Mater. Chem.*, 2011, 21, 5870–5872.
- 36.J. F. Quinn, M. R. Whittaker and T. P. Davis, *J. Controlled Release*, 2015, 205, 190–205.
- 37.E. S. M. Bahnson, H. A. Kassam, T. J. Moyer, W. Jiang, C. E. Morgan, J. M. Vercammen, Q. Jiang, M. E. Flynn, S. I.

- Stupp and M. R. Kibbe, *Antioxid. Redox Signaling*, 2015, 24, 401—418.
- 38.M. Douglass, S. Hopkins, R. Pandey, P. Singha, M. Norman and H. Handa, *Macromol. Biosci.*, 2021, 21, 2000248.
- 39.X. Yao, Y. Liu, J. Gao, L. Yang, D. Mao, C. Stefanitsch, Y. Li, J. Zhang, L. Ou, D. Kong, Q. Zhao and Z. Li, *Biomaterials*, 2015, 60, 130—140.
- 40.T. Yang, A. N. Zelikin and R. Chandrawati, *Adv. Sci.*, 2018, 5, 1701043.
- 41.L. Li, M. Whiteman, Y. Y. Guan, K. L. Neo, Y. Cheng, S. W. Lee, Y. Zhao, R. Baskar, C. H. Tan and P. K. Moore, *Circulation*, 2008, 117, 2351—2360.
- 42.D. E. Discher and A. Eisenberg, *Adv. Hierarchical Nanostruct. Mater.*, 2002, 297, 967—973.
- 43.D. Daubian, J. Gaitzsch and W. Meier, *Polym. Chem.*, 2020, 11, 1237—1248.
- 44.Y. Mai and A. Eisenberg, *Chem. Soc. Rev.*, 2012, 41, 5969—5985.
- 45.I. Khan, K. Saeed and I. Khan, *Arabian J. Chem.*, 2019, 12, 908—931.

- 46.D. Chenthamara, S. Subramaniam, S. G. Ramakrishnan, S. Krishnaswamy, M. M. Essa, F. H. Lin and M. W. Qoronfleh, *Biomater. Res.*, 2019, 23, 20.
- 47.J. W. Yoo, J. S. Lee and C. H. Lee, *J. Biomed. Mater. Res., Part A*, 2010, 92, 1233—1243.
- 48.Y. Zhao, H. Wang and M. Xian, *J. Am. Chem. Soc.*, 2011, 133, 15—17.
- 49.M. C. Urquhart, F. Ercole, M. R. Whittaker, B. J. Boyd, T. P. Davis and J. F. Quinn, *Polym. Chem.*, 2018, 9, 4431—4439.
- 50.Y. Zheng, B. Yu, L. K. De La Cruz, M. R. Choudhury, A. Anifowose and B. Wang, *Med. Res. Rev.*, 2018, 38, 57—100.
- 51.Z. J. Song, M. Y. Ng, Z.-W. Lee, W. Dai, T. Hagen, P. K. Moore, D. Huang, L.-W. Deng and C.-H. Tan, *Med. Chem. Commun.*, 2014, 5, 557—570.
- 52.N. Kayaman-Apohan and Z. S. Akdemir, *Polym. Adv. Technol.*, 2005, 16, 807—812.
- 53.H. Wang, Y. Zhao, Y. Wu, Y. L. Hu, K. Nan, G. Nie and H. Chen, *Biomaterials*, 2011, 32, 8281—8290.
- 54.U. Bilati, E. Allemann and E. Doelker, *J. Microencapsul.*, 2005, 22, 205—214.

- 55.K. L. DeCicco–Skinner, G. H. Henry, C. Cataisson, T. Tabib, J. C. Gwilliam, N. J. Watson, E. M. Bullwinkle, L. Falkenburg, R. C. O'Neill, A. Morin and J. S. Wiest, *J. Vis. Exp.*, 2014, 91, e51312.
- 56.K. Bellacen and E. C. Lewis, *J. Vis. Exp.*, 2009, 33, e1564.

국문 초록

혈관 형성 촉진을 위한 일산화질소와 황화수소 동시 방출 나노입자의 개발

이지은

융합과학부 나노융합전공

융합과학기술대학원

서울대학교

일산화질소와 황화수소는 그들의 다양한 생물학적 기능으로 인해 여러 치료제로의 연구가 주목을 받아왔다. 일산화질소와 황화수소의 제어 방출을 통해 황화수소가 PDE5A를 억제함으로써 일산화질소에 의해 유도되는 혈관 형성을 더 촉진시킬 수 있다. 고분자 기반 전달체는 기체 신호 전달물질을 전달하기 위해 연구되어 왔으며, 일산화질소 및 황화수소의 농도를 조절할 수 있다는 중요한 능력을 가지기 때문에 치료제로써 사용이 되어 왔다. 본 연구에서는, 일산화질소와 황화수소를 동시 방출하는 나노입자를 카르복실 기능화 된 mPEG-PLGH-thiobenzamide [(methoxy poly (ethylene glycol-*b*-lactic-*co*-glycolic-*co*-

hydroxymethyl propionic acid)-thiobenzamide)], PTA copolymer 공중합체로부터 자가조립 방법을 통해 만들었고, diethylenetriamine NONOate (DETA NONOate)를 나노입자 안에 넣었다. FT-IR과 ^1H NMR를 이용해 PTA 공중합체의 구조를 확인했으며, PTA-NO 나노입자는 약 140nm 크기의 core-shell 구조를 갖는 것을 확인했다. PTA-NO 나노입자는 다양한 종류의 세포에서 100% 이상의 생존성을 보여 생체에 적합하다는 것을 입증하였으며, 72시간 동안 지속적으로 일산화질소 및 황화수소를 방출하는 양상을 보였다. 생체 외 실험을 통해 일산화질소와 황화수소를 동시 방출하는 것은 일산화질소 또는 황화수소를 단독으로 방출하는 시험군들에 비해 혈관내피세포에 의한 튜브 형성을 촉진시킴을 확인하였다. 또한 생체 내 실험을 통해 PTA-NO 나노입자가 대조군에 비해 통계적으로 유의미한 차이가 있을 정도의 촉진된 혈관형성을 보임을 증명하였다. 이 결과는 일산화질소 및 황화수소 사이의 상호작용이 의학적으로 응용 가능할 것이라는 타당성을 부여함을 나타낸다.

주요어: 일산화질소, 황화수소, 기능성 mPEG-PLGA, 동시 방출 나노입자, 혈관 형성 촉진

학 번: 2019-21580